Surviving the heavy bombardment: Ancient material at the surface of South Pole-Aitken Basin

Noah E. Petro and Carlé M. Pieters

Department of Geological Sciences, Brown University, Providence, Rhode Island, USA

[1] The oldest, deepest, and largest basin recognized on the lunar surface is the South Pole-Aitken (SPA) basin. In the time since its formation, several processes have modified the original interior of the basin, including the introduction of foreign material by impact basins during the period of heavy bombardment. These later basins redistributed material ballistically across the lunar surface forming a mixed and crushed zone on the scale of about one-kilometer deep. Models of crater excavation, ejected material transport, and mixing during emplacement are used to estimate the amount of foreign material from each basin event introduced into SPA and the degree to which that material mixes with the surface of the interior of SPA. We varied the size of the transient craters for all basins, the degree of mixing between foreign and local material, and the number of basins considered in our evaluation. Our modeling results indicate that materials derived from the original SPA melt breccia comprise at least 15% of the present regolith. The most realistic combinations of model parameters predict a SPA melt breccia component that ranges from 50–80% of the current surface regolith. The compositional character of the SPA interior has apparently not been obliterated by aeons of subsequent basin-forming events.   *INDEX TERMS:* 6250 Planetology: Solar System Objects: Moon (1221); 5420 Planetology: Solid Surface Planets: Impact phenomena (includes cratering); 5470 Planetology: Solid Surface Planets: Surface materials and properties; 5410 Planetology: Solid Surface Planets: Composition; *KEYWORDS:* moon, regolith, South Pole-Aitken Basin

1. Introduction

[2] The South Pole-Aitken (SPA) basin is the largest and oldest recognized impact basin on the Moon [*Stuart-Alexander*, 1978; *Wilhelms et al.*, 1979]. The basin is approximately 2500 km in diameter [*Spudis et al.*, 1994] and is between 6.2 and 8.2 km deep [*Zuber et al.*, 1994; *Cook et al.*, 2002]. Remote sensing studies [*Pieters et al.*, 1997, 2001; *Lucey et al.*, 1998] suggest that the basin may have excavated lower-crust or upper-mantle materials during its formation, making SPA a unique location for examining surficial exposure of rock formed at depth. Multispectral data from both the Galileo and Clementine missions indicated that there may be an enrichment in mafic materials within the basin [*Belton et al.*, 1992; *Head et al.*, 1993; *Lucey et al.*, 1995, 1998; *Pieters et al.*, 2001]. The Lunar Prospector gamma-ray data independently showed that there is an Fe anomaly associated with the basin interior [*Lawrence et al.*, 2002] as well as an observed Th enhancement relative to the surrounding highlands [*Lawrence et al.*, 1998, 2002; *Jolliff et al.*, 2000].

[3] The formation of this large basin is predicted to have created a large amount impact melt [*Cintala and Grieve*, 1994, 1998; *Lucey et al.*, 1998]. The amount of impact melt and melt breccia generated and the distribution of material from depth exposed at the surface are dependent on the shape and size of the transient crater [e.g., *Cintala and Grieve*, 1998; *Croft*, 1985; *Melosh*, 1989]. *Schultz* [1997] utilized gravity studies to conclude that the impact that formed SPA was an oblique one that resulted in excavating upper crustal material. *Wieczorek and Phillips* [1999] reconstructed the depth of excavation and transient crater size from gravity data and also found that the crust beneath SPA is relatively thick indicating a shallow depth of excavation. *Melosh* [1989], *Head et al.* [1999], and *Cintala and Grieve* [1998] rely on proportional scaling models that reconstructs the transient crater of SPA in order to estimate the depth of excavation. These estimates range from excavating mostly upper crust to excavating into the lower crust or upper mantle. Material that has been derived from depth and exposed at the surface can be used to determine the composition of the lower crust or upper mantle. Regardless of the depth of origin for the SPA melt, eons of geologic processes have altered the apparent composition of material from the original SPA interior. In addition, the emplacement of localized mare and pyroclastic deposits have covered some of the original SPA material. This begs the question; does any original deep-seated SPA melt material (what will be referred to here as melt breccia) remain at the surface
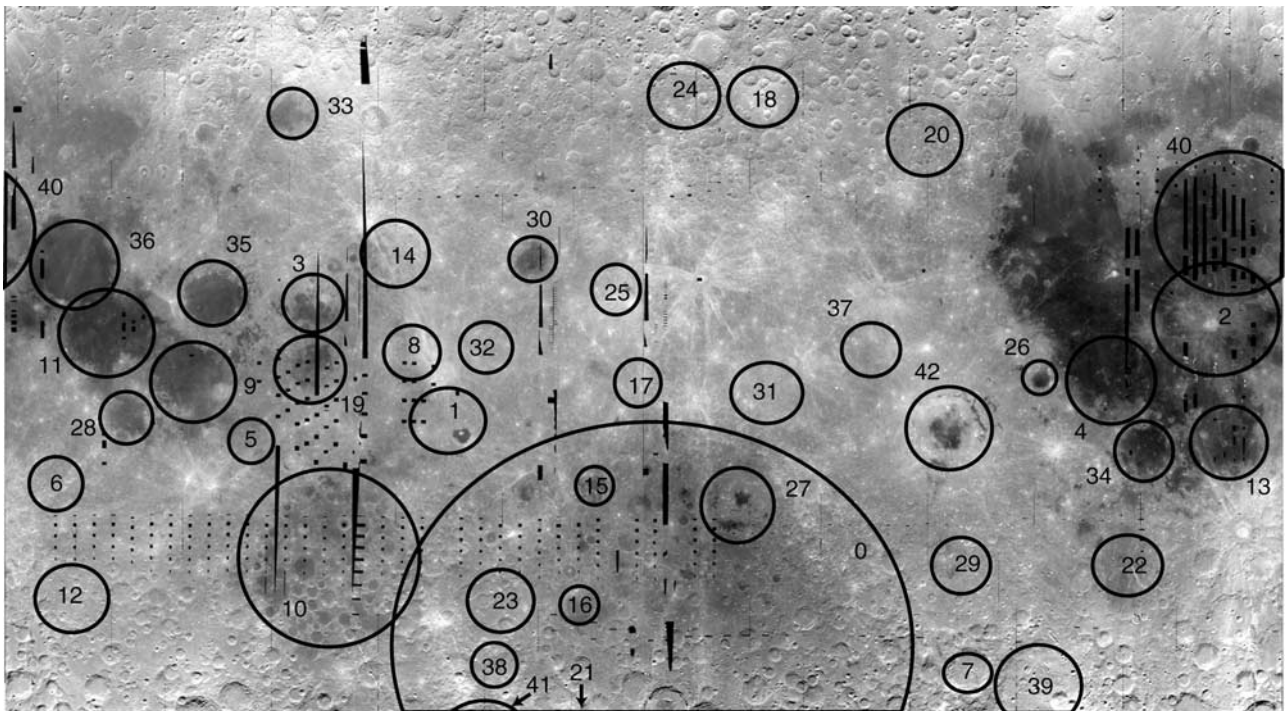
Figure 1. Clementine 750 nm albedo image of the Moon in Mercator projection with latitudes from 70°N to 70°S, centered on 0°N, 180°W. The general locations of basins used in this study are indicated (basins identified by *Spudis* [1993]). Number in each basin refers to number listed in Table 1.

within SPA or have billions of years of geologic processes altered the surface beyond recognition?

[4] We address this issue by evaluating the large-scale lunar-wide lateral redistribution of material solely from basin-forming events and the mixing of foreign material derived from such basins within the SPA regolith, quantitative models for these two processes are used to estimate the relative amount of foreign material that has diluted the original SPA melt breccia derived from the deep interior. Our analyses are independent of the composition(s) of such ancient material.

2. Background

[5] The formation of the large lunar basins occurred over a period of time prior to ~3.8 Ga [*Wilhelms*, 1987; *Ryder*, 2002] during which the lunar megaregolith was formed. Material ejected by the lunar basins mixed ballistically with the surface creating a mixed zone in the upper meters to kilometers of the lunar surface [*Short and Foreman*, 1972; *Arvidson et al.*, 1975; *Hörz et al.*, 1991]. This process occurred across the Moon to varying degrees during the formation of the basins. The basin-forming events involved extensive mixing between the material ejected by the basins and the local surface on which it was emplaced. A location on the lunar surface near a given basin received relatively large amounts of ejected material, while a location some distance away did not receive as much ejected material. The distant ejecta material, however, arrived with a greater velocity than the material closer to the basin. This distal ejecta then underwent a greater degree of mixing and dilution with the local regolith [*Oberbeck et al.*, 1974].

[6] Identifying and cataloging the characteristics and number of basins across the lunar surface has been a research activity since the first lunar orbiting missions [e.g., *Hartmann and Wood*, 1971; *Wilhelms*, 1987; *Pike and Spudis*, 1987; *Spudis*, 1993]. *Hartmann and Wood* [1971] defined basins as having main topographic rims larger than 300 km in diameter. Using the *Hartmann and Wood* [1971] definition for a lunar basin, the *Spudis* [1993] catalog represents a complete examination of lunar basins, including those basins with topographic expressions that have been almost completely erased.

[7] The lunar-wide distribution of basins of varying sizes has implications for the redistribution of material across the Moon. Several studies have modeled this redistribution of materials. *McGetchin et al.* [1973] modeled the distribution of basin ejecta in order to estimate the amount of foreign material at the Apollo landing sites, while *Moore et al.* [1974] used features associated with the Orientale basin to examine the distribution of ejecta by multiringed basins. A map of the basins across the surface of the Moon as identified by *Spudis* [1993] is shown in Figure 1. This distribution allows a qualitative assessment of the modification history due to basins on the lunar surface. Of the 42 basins positively identified by *Spudis* [1993], seven are found within the SPA basin itself and also redistributed materials throughout SPA.

3. Approach

[8] Our approach to evaluate the effects of the basin-forming period of lunar history on the materials within SPA basin involves (1) the estimation of how much material is

introduced into SPA from each lunar basin during the basin-forming period and (2) the degree to which the incoming foreign material is mixed with local surface material within SPA. The amount of foreign material introduced into SPA is dependent on the number of basins considered as well as the size and proximity of these other basins to SPA.

[9] A similar approach was used in evaluating the provenance of materials of the Cayley and Descartes formations sampled during the Apollo 16 mission [e.g., *Hodges et al.*, 1973; *Oberbeck et al.*, 1974]. *McGetchin et al.* [1973] estimated how much total material had been introduced to the Apollo 16 site by several of the nearside basins to create a hypothetical local stratigraphy. This estimation lead to their conclusion that much of the stratigraphic column at the Apollo 16 site could be dominated by foreign material from the Nectaris and Imbrium basins. *Ulrich et al.* [1981] argued that based on the morphology of the Cayley and Descartes terrains, both are linked to the Imbrium event and that Nectaris material is only found at depth. In a finding similar to that of *McGetchin et al.* [1973], *Stöffler* [1985] determined that the Cayley and Descartes terrains have distinct origins based on an analysis of samples from the North Ray crater. The authors postulated that the Cayley terrain was formed by Imbrium ejecta while the older Descartes formation contains Nectaris ejecta. The three approaches (one based on ejecta modeling, one on surficial morphology, and one on sample analysis) provide a framework for understanding the effect of the formation of distant basins on local geology.

[10] *Spudis* [1993] describes 42 basins that are distributed across the lunar surface (see Figure 1). These basins are listed in Table 1 in stratigraphic order [*Wilhelms*, 1987] with their main ring sizes [*Spudis*, 1993]. The spatial relation of these basins to the Apollo 16 site and the size of the basins are illustrated in Figure 2 (distances are from the Apollo 16 landing site to the center of each basin). In order to illustrate the relative ages of the basins, three age groups are identified by different symbols. Of the 42 lunar basins, eight of the ten most recent basins and several of the largest (≥600 km) basins are within 90° of the Apollo 16 landing site. The relationship between large basins, many of which happen to be recent, and the Apollo 16 site certainly suggests that these basins have had a major effect on the local geology.

[11] A different relationship between diameter, and location of these 42 basins is observed for a site in the central region of SPA (60° South, 160° West, to be discussed below). Figure 3 illustrates the spatial relationship between this SPA location and all 42 basins. However, in contrast to the Apollo 16 site, most of the large (>500 km in diameter) and recent basins are located further than 90° from the SPA location (i.e., on the opposite hemisphere). Additionally, most of the basins located within 90° of the SPA location are smaller than 500 km in diameter and several of these basins are located within SPA itself (e.g., Apollo, Ingenii, and Schrödinger). Clearly the effect of the formation of basins on the interior of SPA will be quite different than what dominates the geology at Apollo 16.

## 3.1. Models for Estimating the Modifying Effect of Basin Formation on the Interior of SPA

[12] Models for the distribution of ejecta from craters and basins have been developed based on terrestrial and lunar

Table 1. Lunar Basins[a]

	Basin	Main Ring Diameter, km	Angular Distance
0	South Pole-Aitken	2600	
1	Tsiolkovsky-Stark	700	67.8
2	Insularum	600	122.2
3	Marginis	580	120.0
4	Flamsteed-Billy	570	96.4
5	Balmer	500	95.1
6	Werner-Airy	500	96.3
7	Pingre-Hausen	300	39.6
8	Al-Khwarizmi-King	590	89.6
9	Fecunditatis	690	111.5
10	Australe	880	53.7
11	Tranquillitatis	700	125.2
12	Mutus-Vlacq	690	69.5
13	Nubium	690	94.7
14	Lomonosov-Fleming	620	108.6
15	Ingenii	315	34.9
16	Poincare	325	19.4
17	Keeler-Heaviside	500	56.9
18	Coulomb-Sarton	440	115.5
19	Smythii	740	99.4
20	Lorentz	365	107.1
21	Amundsen-Ganswindt	335	30.1
22	Schiller-Zucchius	335	53.8
23	Planck	325	32.2
24	Birkhoff	325	119.0
25	Freundlich-Sharonov	600	80.5
26	Grimaldi	440	87.0
27	Apollo	480	24.3
28	Nectaris	860	103.6
29	Mendel-Rydberg	420	37.8
30	Moscoviense	420	95.7
31	Korolev	440	55.1
32	Mendeleev	365	80.0
33	Humboldtianum	650	149.3
34	Humorum	425	94.9
35	Crisium	740	129.4
36	Serenitatis	920	147.5
37	Hertzsprung	570	65.9
38	Sikorsky-Rittenhouse	310	36.5
39	Bailly	300	38.3
40	Imbrium	1160	143.8
41	Schrodinger	320	27.5
42	Orientale	930	60.5

[a]Multiringed basins of the Moon defined by *Spudis* [1993] and listed in stratigraphic order [*Wilhelms*, 1987]. Properties listed include angular distance from SPA-1 (in degrees), and main ring diameter from *Spudis* [1993].

craters [*McGetchin et al.*, 1973; *Pike*, 1974] and on impact scaling laws [*Housen et al.*, 1983]. The estimated amount of foreign material introduced into SPA can be calculated for any lunar basin based on these models, but the models do not describe how this foreign material mixes with the local regolith during emplacement. *Oberbeck et al.* [1974, 1975] modeled the interaction of foreign material ejected from a crater with the local surface at a distal location. The *Oberbeck et al.* [1975] model was based on measurements of laboratory produced craters centimeters in size as well as field observations of the secondary craters of Copernicus. This model allows an estimation of the amount of mixing between incoming foreign material from basins and the local regolith. We have combined both types of models to estimate the amount of foreign material introduced into SPA and the mixing ratio of local to foreign basin material that occurred during the period of heavy bombardment. The details of each model are described below. It should be
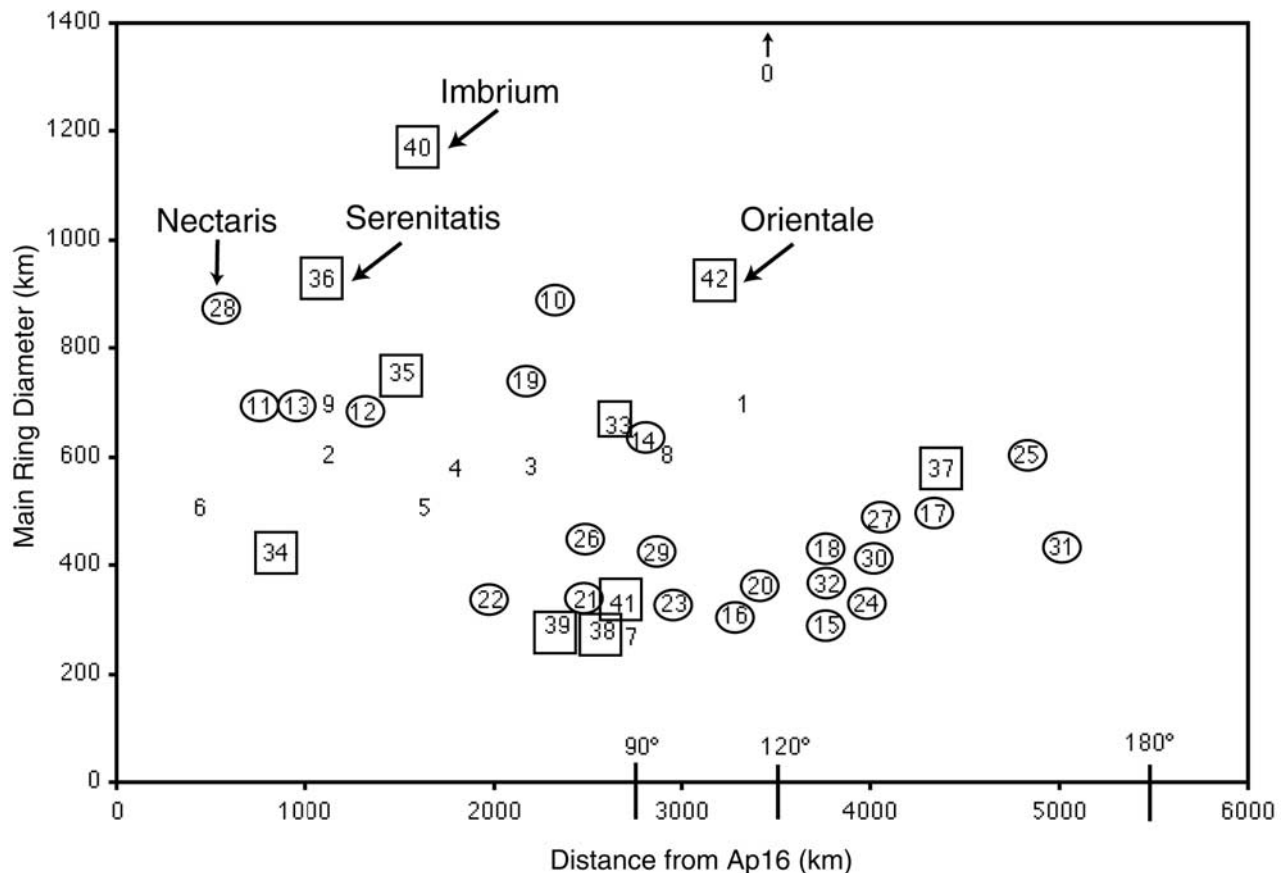
Figure 2. Comparison of the main ring diameters of all lunar basins [*Spudis*, 1993] and their distance to the Apollo 16 landing site. The 10 most recent basin events [*Wilhelms*, 1987] are enclosed in squares, the 22 intermediate aged basins are enclosed in circles, and the 10 oldest are not enclosed. Numbers refer to the basins listed in stratigraphic order [*Wilhelms*, 1987] in Table 1. The SPA basin is indicated by a 0 on this figure.

noted that the smaller craters found throughout SPA and those just outside of the basin will also redistribute material across the surface [e.g., *Haskin et al.*, 2003a; *Li and Mustard*, 2003], although the modifying effects of these craters will not be addressed in this paper.

3.1.1. The Pike Model: Amount of Foreign Material

[13] Following the Apollo lunar missions, *McGetchin et al.* [1973] developed an equation that estimated the radial variation in the thickness of ejecta based on observed ejecta thicknesses from explosion craters, terrestrial craters, laboratory craters, and observations of ejecta from Copernicus and the Imbrium basin. This equation was used to estimate the average contribution of foreign material from the nearside basins to the Apollo landing sites. The calculated thicknesses were then used to estimate the stratigraphy of basin deposits and to determine the provenance of the lunar samples. However, *Pike* [1974] questioned the *McGetchin et al.* [1973] model's estimation of the amount of ejecta at the rim of basins and developed a different estimation that was then incorporated into a revised ejecta thickness model. Overall, the revised *Pike* [1974] equation estimates greater amounts of ejected material than the *McGetchin et al.* [1973] model. Similarly, the *Pike* [1974] equation predicts approximately 2–3 times greater thicknesses of ejected

material than the *Housen et al.* [1983] model (when using the value of the coefficient A advocated by *Wieczorek and Zuber* [2001]). Although we principally use the Pike model here, we compare results from the Pike model with results of the Housen model.

[14] In the analysis presented here, the estimated average amount of ejected material at any given distance from a basin is calculated using the equation from *Pike* [1974]

$$t = 0.033\,R\,(r/R)^{-3.0} \qquad (1)$$

where t is the thickness of material ejected from the basin at a location r meters from the center of the basin and R is the radius of the transient crater (TC).

[15] There are several issues that the *Pike* [1974] model does not account for and need to be addressed. For example, the model does not take into account the curvature of the lunar surface, therefore a correction factor based on the radial distance from the basin to the location of interest should be applied to the calculated thickness value in order to account for antipodal thickening of ejecta [e.g., *Moore et al.*, 1974; *Wieczorek and Zuber*, 2001]. The model does not distinguish between the continuous ejecta deposits sur-
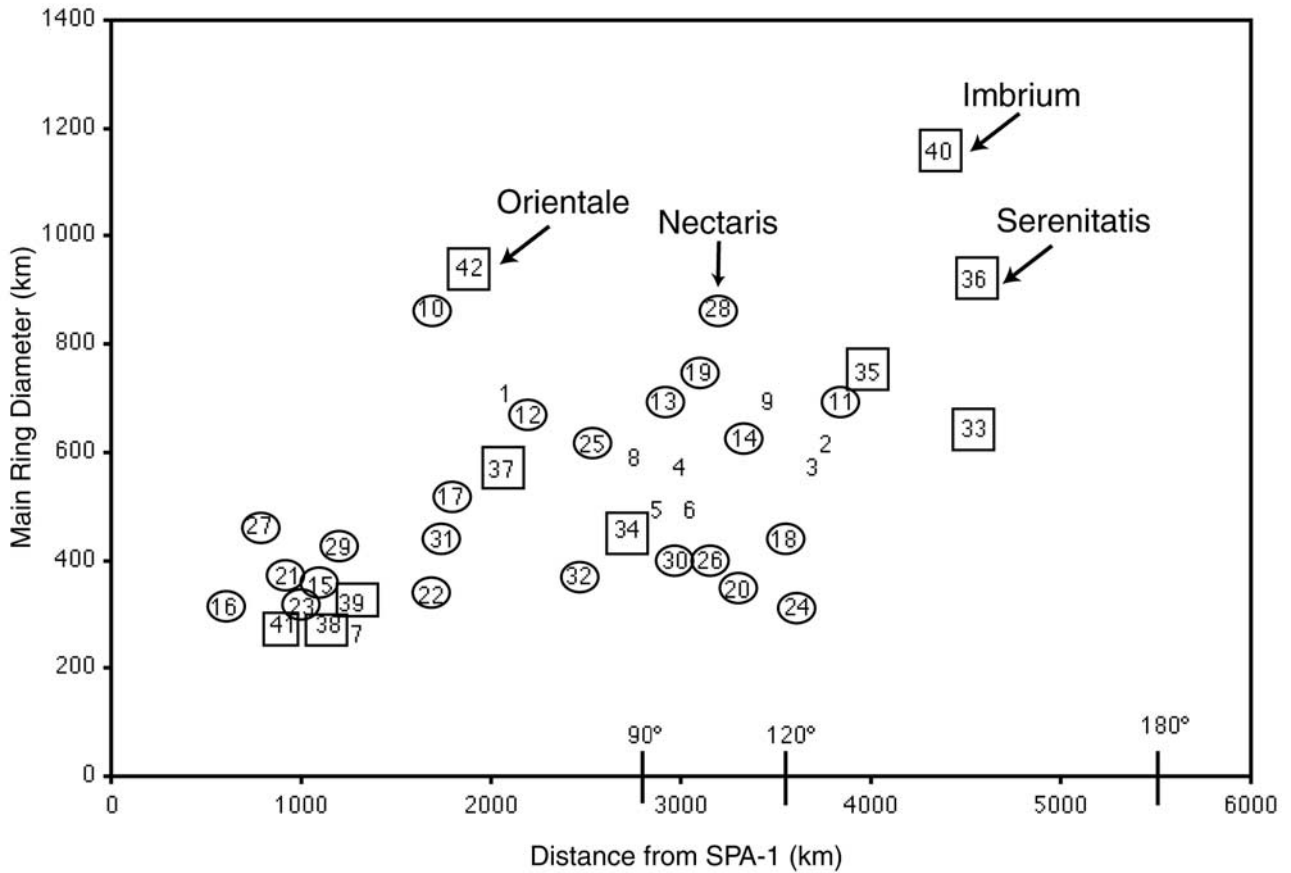
Figure 3. Comparison of the main ring diameters of all lunar basins [*Spudis*, 1993] and their distance to SPA-1. The 10 most recent basin events [*Wilhelms*, 1987] are in squares, the 22 intermediate aged basins are enclosed in circles, and the 10 oldest are not enclosed. Numbers refer to the basins listed in Table 1.

rounding a basin and the discontinuous ejecta deposits at distal locations. Equation (1) also assumes a vertical impact formed the basins, resulting in a uniform distribution of ejecta around each basin. This issue, as well as the likely variation in amount of material deposited outside of the continuous ejecta deposits, will be accommodated with parameter variation in a subsequent section. Despite these shortcomings, the *Pike* [1974] equation is useful in estimating how much foreign material lunar basins excavate and distribute elsewhere, and in particular into SPA.

3.1.2. Oberbeck Local Mixing Hypothesis

[16] Following the Apollo 16 mission, the significance of lunar basin ejecta on the modification of the lunar surface was appreciated in much better detail [*Hodges et al.*, 1973]. Materials ejected from basins and craters mix with and remobilize the lunar regolith. This mixing process was addressed analytically by *Oberbeck et al.* [1975], where they found that the amount of local material at a distal location is typically greater than the amount of foreign material ejected from the crater. The ejected material is emplaced and mixed with local materials. This led to the conclusion that regoliths that have been affected by foreign materials ballistically emplaced as ejecta from a distal crater will be composed of primarily local material. A mixing ratio (μ) for a single location defined by *Oberbeck et al.* [1975] is the ratio of local material that is mixed with foreign material

that has been ballistically ejected from a basin or primary crater. The estimated μ value is given by the equation

$$\mu = 0.0183 * R_S^{0.87} \qquad (2)$$

where R_s is the distance from the location of interest to the center of the impact event.

[17] The largest observed μ values reported by *Oberbeck et al.* [1975] were at 600 km from Copernicus with a corresponding μ value of approximately 5.00. Several subsequent studies tested the accuracy of the μ calculation in lunar settings using independent spectral mixing models and remote sensing data. *Pieters et al.* [1985] examined mixing relationships along a ray of Copernicus between feldspathic ejecta and the mare substrate and found that the mixing ratio calculated by equation (2) agrees with mixing measurements made using remote sensing data. It was also found that the mixing ratio as determined by equation (2) appears to overpredict the amount of mixing within 3 crater radii. *Head et al.* [1993] examined the mixing relationship between ejected feldspathic material from Orientale and basaltic plains in the Schiller-Schickard region using Galileo SSI data. The μ values calculated using a spectral mixing model range from 1.09 to 3.27 and are within a factor of 1.5 of the μ values predicted *Oberbeck et al.* [1975]. Similarly, *Blewett et al.* [1995], using Earth based
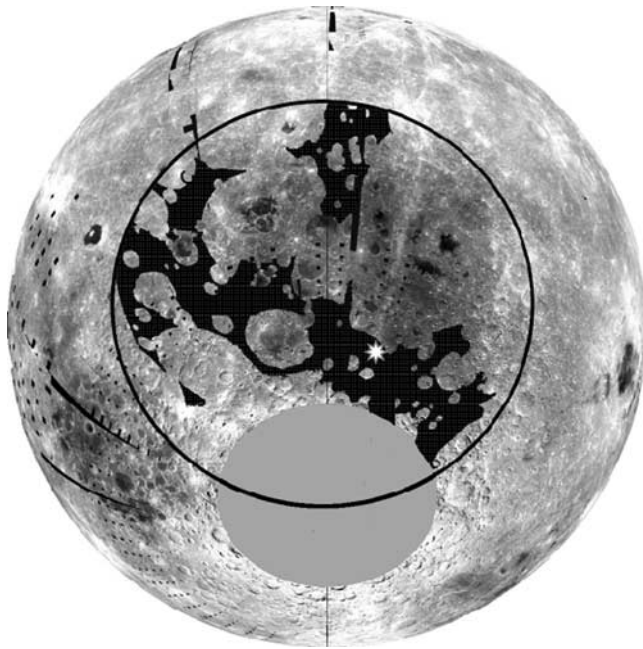
Figure 4a. Orthographic projection of Clementine 750 nm albedo image. The image is centered on 180°W, 50°S, a previously proposed SPA center [*Wilhelms*, 1987]. Circle outlines main ring of SPA as identified by *Wilhelms* [1987]. Terrain in stipple pattern is identified as being "Interior Materials of South Pole-Aitken Basin." Star is location of SPA-1 at 160°W, 60°S.

telescopic spectra of the Schiller-Schickard region, found that the *Oberbeck et al.* [1975] mixing model agrees with or may slightly overestimate the amount of local material (Schiller-Schickard mare) involved in mixing with feld-spathic material from Orientale. The possible overestima-tion may be due to factors not directly related to the *Oberbeck et al.* [1975] model including possible contami-nation of the Schiller-Schickard cryptomare by highland material from subsequent local, smaller impacts or the type of spectral mixing model used. These spectral mixing studies found μ values from 1.50 to approximately 5.00 for the Schiller-Schickard cryptomare, values that generally agree with μ values calculated from equation (2). In sum-mary, spectral mixing models tend to confirm the model formulated by *Oberbeck et al.* [1975] for μ values up to 5.00, but no data exist for larger values.

3.2. Example Site Within SPA

[18] The above models can be used to estimate how much material derived from the original SPA interior remains in the surface regolith at any site within SPA following the basin-forming events that created much of the megaregolith. However, some of the interior of SPA has clearly been modified by other processes such as volcanism (although not as extensive as nearside volcanism). Several isolated mare deposits have been identified throughout the interior of SPA [*Stuart-Alexander*, 1978; *Wilhelms et al.*, 1979; *Yingst and Head*, 1999]. Additionally, a few areas of smooth plains located in the central region of SPA have been interpreted as containing cryptomare deposits [*Pieters et al.*, 2001].

[19] We have selected a site that is outside of the identified mare and cryptomare deposits and is in terrain that has been mapped as possibly containing ancient mate-rials. This specific location will be referred to as SPA-1 and is located at 60°S, 160°W near a proposed center of SPA at 56°S, 180°W [*Wilhelms et al.*, 1979]. Geologic maps of the interior of SPA [*Stuart-Alexander*, 1978; *Wilhelms et al.*, 1979] include terrains described as being pre-Nectarian in age. Synthesizing several of these Pre-Nectarian units, *Wilhelms* [1987] described a terrain in SPA as containing "Interior Materials of South Pole-Aitken Basin." This ancient terrain is illustrated in Figure 4a and excludes mare deposits as well as the continuous ejecta deposits of basins within and around SPA. The selected example site is located within the identified Pre-Nectarian terrain and is indicated by a star in Figure 4a. The region surrounding SPA-1 is shown in Figure 4b, with the materials outside of the ancient terrain shaded and SPA-1 identified by a star.

[20] At SPA-1 we have calculated the amount of foreign material introduced into SPA by each of the 42 basin events (Table 1) and the mixing of that material with the local surface. Previous work [*Petro and Pieters*, 2003] used a similar area in preliminary studies. Identified mare and cryptomare deposits are located ~150 km from SPA-1 and may have contributed some material to the site through smaller, more local impacts. Spectral mixing analysis of this location [*Gillis et al.*, 2003] suggests that material derived from the mare and cryptomare deposits may comprise up to 20% of the regolith at SPA-1. On the basis of the afore-mentioned series of observations of the SPA-1 region, it is likely that this example site (SPA-1) experienced minimal resurfacing other than the mixing of later basin materials with the local regolith, making it an acceptable location to conduct this study.

3.3. Range of Model Parameters Investigated

[21] Simply applying each of the above models to predict basin contributions to SPA-1 will produce a single value for the percent of ancient SPA melt breccia that remains at the surface of SPA. However, since there is considerable uncertainty inherent in each of the models, we varied the
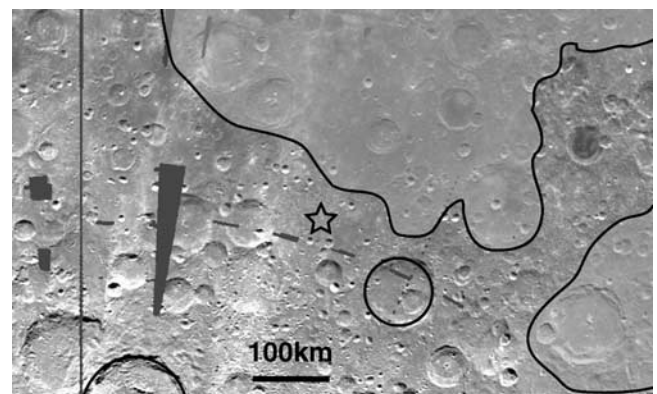
Figure 4b. The region immediately surrounding SPA-1 of "Interior Materials of South Pole-Aitken Basin" mapped by *Wilhelms* [1987]. SPA-1 location is marked with a star. The shaded region combine units mapped as mare material and Apollo basin ejecta. Vertical line at left is 180°W.
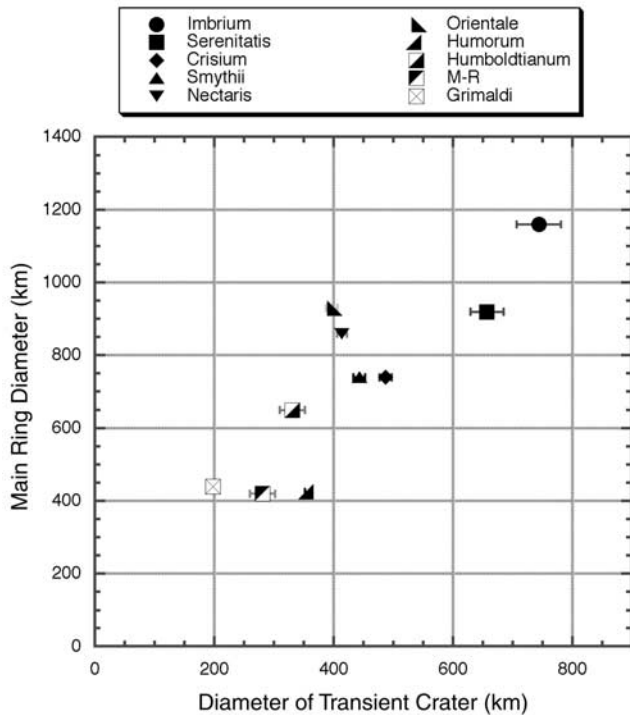
Figure 5a. Estimated transient crater sizes for 10 lunar basins from *Wieczorek and Phillips* [1999] compared to the main ring diameter from *Spudis* [1993]. Note that some of the symbols are larger than their estimated error bars.

model parameters and the number of basins considered in order to evaluate several possible scenarios. The range of values from these scenarios can be used to examine what may have occurred during the basin-forming period of lunar history. These options allow us to develop realistic expectations for the regolith within SPA.

[22] As mentioned previously, we include basins described by *Spudis* [1993] and the stratigraphic sequence of *Wilhelms* [1987] in our calculations. The basins are considered in three groups based on their distances from SPA-1 to the center of each basin. The first group of basins involves all 42 basins in stratigraphic sequence. The second group used basins with centers located within 120° of SPA-1. In considering this group of basins any possible effects of antipodal ejecta thickening from the large nearside basins [e.g., *Moore et al.*, 1974; *Wieczorek and Zuber*, 2001] are effectively removed. The third group uses basins with centers located within 90° of SPA-1 (i.e., are on the same hemisphere). This group excludes most of the nearside basins from consideration and therefore eliminates the uncertainty of very distant basin deposits.

[23] The transient crater (TC) size is a very important variable in the ejecta thickness equation (equation (1)) and determines the amount of foreign material introduced to SPA-1. The variation of this parameter might accommodate some of the expected spatial variations in the amount of material ejected by a basin and introduced into SPA. To estimate the TC size, we have relied heavily on the work of *Wieczorek and Phillips* [1999] who used geophysical data from the Clementine mission to define TC sizes for 11 lunar

basins, including SPA. In their study, only basins larger than ~365 km in diameter were considered, which corresponds to the approximate resolution of the then available gravity model. Furthermore, basins as old as Tranquillitatis were excluded as the Moho uplift beneath these basins was found to be significantly less than the youngest basins. The observed degraded morphology could either be a result of crustal viscous relaxation or the infill of the crater by basin ejecta. In order to obtain values for the size of the TC for all 42 lunar basins, we developed a method for estimating TC size based on main ring size, but constrained by the *Wieczorek and Phillips* [1999] results.

[24] The TC diameters derived by *Wieczorek and Phillips* [1999] are shown in Figure 5a for 10 basins. These TC sizes are compared with the size of the basin using the observed main ring diameter of *Spudis* [1993]. Note that there is a general, but highly variable, relation between TC size and main ring diameter. This mean trend is shown as a heavy dashed line in Figure 5b. The individual TC and main ring sizes that lie furthest from the mean trendline of the *Wieczorek and Phillips* [1999] data in Figure 5a are identified by stars in Figure 5b. A range of possible TC sizes (minimum, mean, and maximum) is estimated for topographic ring sizes larger than 300 km in diameter. The minimum, mean, and maximum values are illustrated in Figure 5b. For the calculations discussed below, we used these size estimates as a group and did not mix different types of estimates. In other words, a group of calculations were performed using only the minimum TC size, or the mean, or the maximum for all basins involved. In addition to the minimum, mean and maximum TC size, a composite
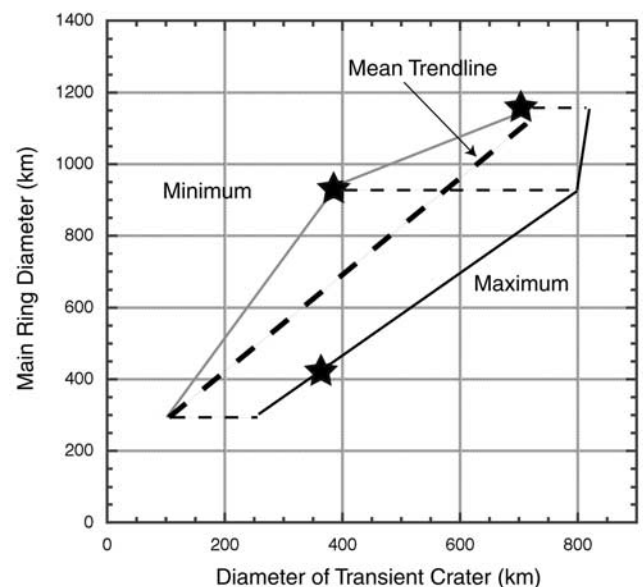
Figure 5b. Relation of transient crater (TC) sizes to main ring diameter used to estimate the minimum, mean, and maximum TC diameters for 42 basins. The mean trend from Figure 5a is shown as a heavy dashed line. Data (plus error estimates) from *Wieczorek and Phillips* [1999] farthest from the mean trend are marked with a star and were used to define the ranges used for minimum and maximum values for other basins.

Table 2. Example Sequence of Calculations[a]

Basin	Mean TC Diameter Estimation, km	μ/2	Foreign Material, m	DoM_i, m	$L\text{-}SPA_i$
Tsiolkovsky-Stark	409	7	8.5	59	85.7
Insularum	330	12	1.2	14	78.3
Marginis	315	11	1.0	12	71.5
Flamsteed-Billy	307	9	1.2	12	64.0
Balmer	252	9	0.6	5	57.2
Werner-Airy	252	9	0.6	5	51.1
Pingre-Hausen	95	4	0.1	0.5	39.4
Al-Khwarizmi-King	322	9	1.7	15	56.2
Fecunditatis	401	11	2.9	31	64.4
Australe	550	6	50.9	290	78.1
Tranquillitatis	409	12	2.8	33	71.6
Mutus-Vlacq	401	7	7.4	53	63.6
Nubium	401	9	3.7	35	56.8
Lomonosov-Fleming	346	11	1.7	17	51.4
Ingenii	107	4	0.2	1	38.3
Poincare	115	2	1.8	4	27.8
Keeler-Heaviside	252	6	1.9	11	35.7
Coulomb-Sarton	205	11	0.2	2	32.5
Smythii	440	10	5.0	48	47.4
Lorentz	146	10	0.1	1	42.9
Amundsen-Ganswindt	122	3	0.6	2	32.8
Schiller-Zucchius	122	6	0.1	1	27.1
Planck	115	4	0.4	1	21.8
Birkhoff	115	11	0.02	0.2	19.9
Freundlich-Sharonov	330	8	2.4	19	39.4
Grimaldi	205	9	0.3	3	34.8
Apollo	236	3	16.5	47	51.2
Nectaris	534	10	10.1	102	51.2
Mendel-Rydberg	189	4	1.9	8	39.0
Moscoviense	189	9	0.2	2	34.8
Korolev	205	6	0.9	5	31.2
Mendeleev	146	8	0.1	1	27.3
Humboldtianum	369	14	2.1	29	43.0
Humorum	193	9	0.2	2	38.4
Crisium	440	12	3.7	46	42.0
Serenitatis	581	14	12.6	173	55.5
Hertzsprung	307	7	2.9	20	47.4
Sikorsky-Rittenhouse	103	4	0.2	1	35.7
Bailly	95	4	0.1	1	27.3
Imbrium	769	13	37.1	479	73.2
Schrodinger	111	3	0.6	2	50.2
Orientale	589	6	48.8	308	61.5

[a]Example of the sequence of calculations for each basin required for scenario # 43 of Table 3. This scenario used all multiringed lunar basins, the μ/2 value, and the mean transient crater estimation. The μ value is calculated from equation (2) and the estimation of the foreign material is based on equation (1).

mean (mean*) size is also used. The mean* size includes the predicted size of the TC for the ten basins (not including SPA) as discussed by *Wieczorek and Phillips* [1999] and the mean size for the remaining 32 basins.

[25] As mentioned previously, spectral mixing studies appear to have validated the *Oberbeck et al.* [1975] mixing ratio μ up to a value of 5.00 [*Pieters et al.*, 1985; *Head et al.*, 1993; *Blewett et al.*, 1995]. However, at SPA-1 the μ value for many basins exceeds 5.00 considerably. Therefore the μ parameter is varied systematically in order to observe the effects that the degree of mixing has on the resulting composition of the regolith. In discussing the ratio of local to foreign material, the variable μ′ will be used for the remainder of the paper to define the concept of the mixing ratio as described by *Oberbeck et al.* [1975] while μ is the mixing ratio as explicitly defined by equation (2). The first estimate uses the standard μ value calculated from equation (2). We note, however, that some model calculations using the standard value for μ for large basins predicts

a mixed zone on the nearside on the order of ∼50 km resulting from SPA itself. Such a depth of mixing is much larger than most estimates of the mega-regolith by almost an order of magnitude. Therefore three additional values for the μ′ parameter are used to accommodate the uncertainty in μ′ and to assure that the megaregolith is reasonably bounded. The second μ′ estimate uses the value of μ/2, while the third estimate uses μ/4. The fourth estimate modifies all μ values greater than 10.0 by reducing them by half of their difference from 10.0 (e.g., if μ = 25.0, then modified μ′ = 17.5), this adjustment attempts to address the possibility that very large calculated μ values are overestimated while values of 10.0 and below are less uncertain.

[26] All variations of the parameters mentioned above are combined to generate 48 different scenarios that describe the basin forming period. The TC size estimates are used in equation (1) and result in various estimations of how much foreign material is introduced to SPA-1. These estimations are then used with the various μ′ parameters to describe

Table 3. Calculated Scenarios[a]

Scenario	Number of Basins	TC Estimate	μ' Used	Total Foreign Material, m	DoM_t, m	$L\text{-}SPA_t$
1	120 degrees	Max TC Size	Modified μ	931.3	2542.42	65.78
2	120 degrees	Max TC Size	μ	931.3	2006.58	65.87
3	120 degrees	Max TC Size	$\mu/2$	931.3	1003.24	46.24
4	120 degrees	Max TC Size	$\mu/4$	931.3	501.64	24.16
5	120 degrees	Mean * TC Size	Modified μ	139.04	616.64	47.8
6	120 degrees	Mean * TC Size	μ	139.04	651.92	51.5
7	120 degrees	Mean * TC Size	$\mu/2$	139.04	362.25	28.2
8	120 degrees	Mean * TC Size	$\mu/4$	139.04	217.42	10.39
9	120 degrees	Mean TC size	Modified μ	174.66	552.45	73.75
10	120 degrees	Mean TC size	μ	174.66	616.84	76.21
11	120 degrees	Mean TC size	$\mu/2$	174.66	308.42	58.63
12	120 degrees	Mean TC size	$\mu/4$	174.66	154.21	34.4
13	120 degrees	Min TC size	Modified μ	40.38	131.17	69.69
14	120 degrees	Min TC size	μ	40.38	114.95	72.01
15	120 degrees	Min TC size	$\mu/2$	40.38	57.47	53.46
16	120 degrees	Min TC size	$\mu/4$	40.38	28.74	30.1
17	90 degrees	Max TC Size	Modified μ	809.07	2450.83	66.12
18	90 degrees	Max TC Size	μ	809.07	2006.58	68.78
19	90 degrees	Max TC Size	$\mu/2$	809.07	1003.29	49.06
20	90 degrees	Max TC Size	$\mu/4$	809.07	501.64	25.48
21	90 degrees	Mean * TC Size	Modified μ	116.86	599.71	54.8
22	90 degrees	Mean * TC Size	μ	116.86	635	58.3
23	90 degrees	Mean * TC Size	$\mu/2$	116.86	345.33	34.2
24	90 degrees	Mean * TC Size	$\mu/4$	116.86	200.5	12.4
25	90 degrees	Mean TC size	Modified μ	148.33	552.45	76.58
26	90 degrees	Mean TC size	μ	148.33	616.84	78.77
27	90 degrees	Mean TC size	$\mu/2$	148.33	308.42	61.99
28	90 degrees	Mean TC size	$\mu/4$	148.33	154.21	37.34
29	90 degrees	Min TC size	Modified μ	34.54	126.65	72.49
30	90 degrees	Min TC size	μ	34.54	114.95	74.92
31	90 degrees	Min TC size	$\mu/2$	34.54	57.47	56.85
32	90 degrees	Min TC size	$\mu/4$	34.54	28.74	32.39
33	All	Max TC Size	Modified μ	1075.84	2673.72	61.16
34	All	Max TC Size	μ	1075.84	2006.58	63.25
35	All	Max TC Size	$\mu/2$	1075.84	1003.29	42.98
36	All	Max TC Size	$\mu/4$	1075.84	501.64	20.41
37	All	Mean * TC Size	Modified μ	204.02	607.33	69.12
38	All	Mean * TC Size	μ	204.02	869.51	75.24
39	All	Mean * TC Size	$\mu/2$	204.02	445.37	57.78
40	All	Mean * TC Size	$\mu/4$	204.02	228	34.64
41	All	Mean TC size	Modified μ	235.21	732.04	72.34
42	All	Mean TC size	μ	235.21	1044.14	78.07
43	All	Mean TC size	$\mu/2$	235.21	546.75	61.47
44	All	Mean TC size	$\mu/4$	235.21	298.05	38.57
45	All	Min TC size	Modified μ	71.63	495.96	81.16
46	All	Min TC size	μ	71.63	718.34	84.89
47	All	Min TC size	$\mu/2$	71.63	363.93	72.37
48	All	Min TC size	$\mu/4$	71.63	186.73	51.8

[a]Summary of the 48 scenarios calculated here. Parameters required in calculating the amount of ancient material at the present surface of SPA-1 are identified for each of the 48 scenarios (see text). The total amount of foreign material introduced to the SPA-1 site, total depth of mixing (DoM_t), and the final estimated amount of material derived from the SPA melt breccia ($L\text{-}SPA_t$) are given for each of the scenarios.

local mixing within SPA. These calculations, which are described below, are done for each of the three basin groups.

3.4. Calculation of Local/Foreign Material From Multiple Events

[27] For all scenarios, equation (1) is used to estimate the amount of foreign material (in meters) introduced into the SPA-1 site by each basin. The calculated value is then corrected to account for the curvature of the Moon. The megaregolith developed from each basin-forming event is examined individually. Each basin event (E_i, where i refers to a basin in Table 1) is considered in the stratigraphic sequence defined by *Wilhelms* [1987]. Starting with the first post-SPA basin event, the calculated amount of foreign material (t_i) introduced to a location (SPA-1) is

multiplied by the mixing ratio μ'_i to obtain the depth of mixing (DoM_i), which is the maximum depth of local material mixed with the incoming foreign material for that particular event.

[28] In order to calculate the amount of original SPA melt breccia remaining in the present regolith at SPA-1, each basin event (E_i) is treated individually. The percentage of local SPA material in the mixed regolith following E_i is given by $L\text{-}SPA_i$,

$$L\text{-}SPA_i = C_i * \left[(\mu'_i - 1)/\mu'_i \right] * 100 \qquad (3)$$

where C_i represents the average composition of the regolith throughout the mixed zone for that event. This $DoM_i = t_i * \mu'_i$. The $L\text{-}SPA_i$ value is calculated for each E_i using the

cumulative results from all previous basin events as starting conditions. For subsequent basin events, the DoM_i value for that event will determine the character of the starting material (C_i) to be used in equation (3). Each basin event creates a new mixed zone (DoM_i) that will consume all or only part of previous mixed zones.

[29] For example, prior to the first post-SPA event (E_1) the composition of material (C_1) at the surface is L-SPA$_0$, or 1.00 (100%) local SPA material. L-SPA$_1$ is therefore simply $[(\mu_1' - 1)/\mu_1'] \times 100$, and DoM_1 is $t_1 \times \mu_1'$. If DoM_{i+1} for subsequent events is less than the DoM_i preceding it, then the method for calculating L-SPA$_{i+1}$ is similar to what was calculated for E_1. The value for C_{i+1}, the composition of material throughout DoM_{i+1}, is simply L-SPA$_i$.

[30] On the other hand, when the DoM_{i+1} of an event is greater than the DoM_i prior to it, the calculation of L-SPA$_{i+1}$ is slightly different. In this case the calculation of the bulk C_{i+1} must take into account all the different mixed zones that comprise the depth of mixing by combining the relative contribution of each. In other words, C_{i+1} is the weighted average of all the L-SPA$_i$ contained within the DoM_{i+1}.

[31] These calculations are performed for each basin event in sequence leading up to the most recent deposition and mixing event. Ultimately the final basin event controls the amount of material derived from the SPA melt breccia at the present surface (L-SPA$_t$). Throughout all basin events, the greatest DoM_i is defined to be the total depth of mixing (DoM_t) for the basin-derived megaregolith.

[32] An example of the sequence of calculations is shown in Table 2 for mean values of the TC, μ' values of $\mu/2$, and all 42 basins (scenario #43 in Table 3). Perhaps the most significant basin events are those that excavate through several zones that have been previously mixed prior to it. These homogenizing events, such as Australe, Imbrium, and Orientale effectively increase the L-SPA$_i$ values. The significance of such events is apparent with the Imbrium example, as the prior L-SPA value is 27.3% while after the Imbrium event L-SPA increases to 73.2%. It should be noted that applying the *Housen et al.* [1983] model for estimating ejecta thickness in this sequence does not significantly change the L-SPA$_t$ value (62.8% versus 61.5%). The reason for this is because the relative scale of mixing is largely dependent on the relative size and distance of the basins involved. On the other hand, the total amount of foreign material and the DoM_t calculated using the *Housen et al.* [1983] model are approximately 1.7 times less than values calculated using the *Pike* [1974] model.

4. Results

[33] An estimation of the amount of ancient material derived from the original SPA melt breccia in the present surface regolith is dependent on the parameters that have been described in section 3.1: the number of basins, the TC size (and therefore ejecta amount), and the mixing ratio μ'. The predicted amount of remaining SPA melt breccia material also depends on the specific location within SPA.

[34] The 48 possible scenarios and the calculations from each with different parameter values were selected to
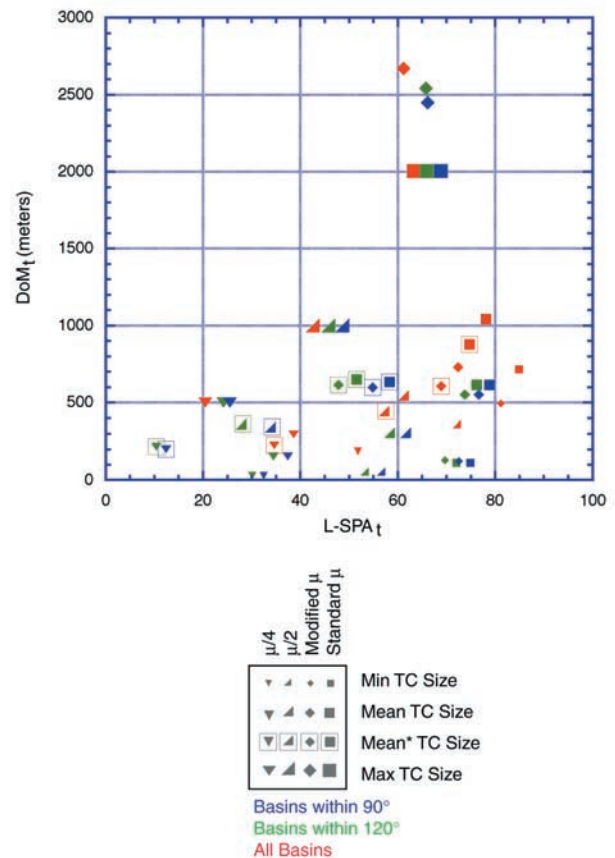

Figure 6. The percentage of SPA-derived material in the present regolith (L-SPA$_t$) and the corresponding depth of mixing (DoM_t) for each of the 48 scenarios. Colors represent each of the three groups of basins examined (red, all basins; green, basins $120°$ from SPA-1; blue, basins $90°$ from SPA-1). The size of each symbol relates to the transient crater size used in each scenario. Values for μ' are represented by differently shaped symbols.

illustrate the effects of different assumptions on the amounts of ancient SPA melt breccia that could be found in the surface regolith today. Table 3 summarizes the parameters used in each scenario, the cumulative amount of foreign material introduced into SPA-1, the total depth of mixing (DoM_t), and the final percent of original SPA material at the surface (L-SPA$_t$).

[35] A comparison of the calculated DoM_t and L-SPA$_t$ is shown in Figure 6 to illustrate the differences between each of the calculated scenarios. The estimated amount of ancient SPA melt breccia material varies from 10 to 86% and the DoM_t zone varies from 28 to 2482 m. This range of scenarios is presented in order to evaluate the effects of different parameters on the results. Some combinations are likely to be more realistic than others.

[36] To more easily discern the effects of different parameters, a subset of Figure 6 is shown in Figure 7 for all scenarios using basins located within $120°$ of SPA-1. Note that with an increasing mixing ratio μ' value (from $\mu/4$ to the standard μ) the amount of SPA material in the surface regolith and the depth of mixing both increase. This relationship is true for all scenarios except for the ones
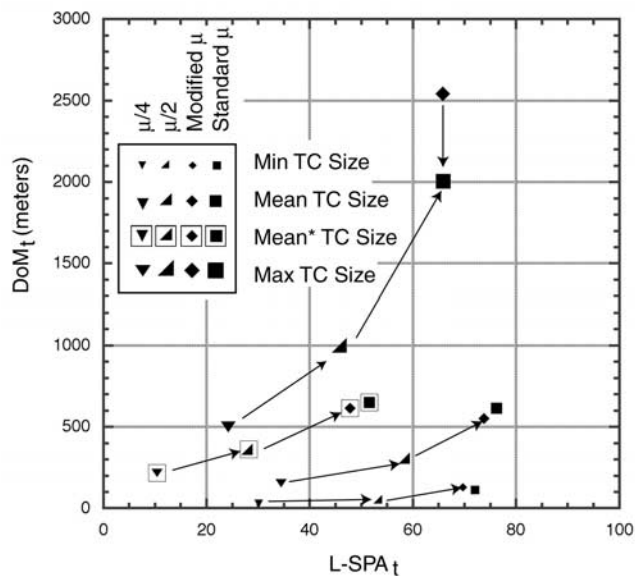
Figure 7. A subset of Figure 6 containing the scenarios involving the basins located within 120° of SPA-1. Arrows indicate the trend for increasing μ' value.

using the maximum TC sizes. Also, with increasing estimated TC size, the calculated DoM_t increases. The variation in the number of basins used (illustrated in Figure 6) does not appear to have a strong effect on the estimated amounts of SPA material in the surface regolith or on the DoM_t values.

5. Discussion

[37] Many of the scenarios listed in Table 3 that use moderate values of the variables (the mean and mean* TC sizes and the standard μ and modified μ values for the μ' value) predict a cumulative DoM_t (megaregolith) from the basin impacts of approximately 500 to 1000 m. This moderate range of values for the variables also predicts that approximately 50–80% of the present regolith will consist of materials derived from the SPA melt breccia. The scenarios that use smaller estimates of the mixing ratio (e.g., $\mu/2$ and $\mu/4$) are expected to substantially underpredict the actual mixing ratio. All but one of the remaining standard μ and modified μ scenarios predicts that 50% or greater of the regolith will be derived from the SPA melt breccia.

[38] In a recent study, *Haskin et al.* [2003a] also calculated the percent of SPA floor material in the present regolith for the same region considered here. They evaluated the effects of nine basins and the nearby crater Bhabha on the composition of the regolith. In addition to a different group of basins, the *Haskin et al.* [2003a] study used the scaling laws of *Housen et al.* [1983] and utilized a different approach as described in *Haskin et al.* [2003b] in calculating the proportion of foreign material from each individual crater or basin event mixed into the present regolith. Despite the differences in approach, their results are quite similar to those presented here. They concluded that approximately 80% of the regolith would have been derived from the original SPA floor.

[39] In considering the depth of the megaregolith formed by the basin events, the scenarios that use the maximum TC size are the only scenarios that result in a DoM_t that is greater than a kilometer (Figure 6). Furthermore, a two-kilometer deep regolith is only formed when the mixing ratio value used is close to the value of μ predicted by *Oberbeck et al.* [1975] (equation (2)) (i.e., standard μ or modified μ). Recall, however, that this DoM_t refers to only the component of megaregolith resulting from basin-scale events post SPA; large local cratering events can also increase the depth of mixing.

[40] The age sequence of basin and their distance from a particular area on the Moon affect the regolith modification history of any particular site. The observed spatial relationships of all basins to SPA-1 is quite different from that seen at the Apollo 16 site (Figures 2 and 3). Four of the most recent and large basins are within 90° of the Apollo 16 landing site. In contrast, the SPA-1 site is greater than 120° from many of the large and recent basins, Serenitatis and Imbrium in particular. The Orientale basin is the only close and large basin to SPA-1. Recall that the mixing ratio μ' variable is dependent only on distance, and thus these large and distant basins also have the highest μ' values (e.g., see Table 2) for SPA-1. Most of the basins that are located within 90° of SPA-1 are smaller than 600 km in diameter and are not among the oldest basins on the Moon (Figure 3). Therefore based on the proximity of the Apollo 16 site to the recent large basins, we might expect that there would be a significantly higher proportion of foreign to local material and that the DoM_t would be greater than found at the SPA-1 site. Calculations for the Apollo 16 site using the methods described here and the same parameters used in Table 2 yields a substantially thicker mega-regolith depth ($\sim$2000 m) than at SPA-1 and only approximately 29% ancient material at the surface. In other words, the Apollo 16 regolith is predicted to be dominated by 71% foreign basin material (70% of which is derived from the Nectaris, Serenitatis, and Imbrium events). This comparison between the Apollo 16 and SPA-1 regolith gives some context for the values calculated for the SPA-1 site.

[41] Despite the spatial and temporal distribution of lunar basins, there are no major variations in either the DoM_t or the amount of SPA melt breccia at SPA-1 due to the number of basins used in our calculations (Figure 6). For most scenarios, the Orientale event is perhaps the most significant as it was the last basin event to occur and it is large and somewhat close to SPA-1. Its proximity indicates that it will introduce a comparably large amount of material to SPA-1 (Table 2) while still having a mixing ratio value larger than many other basins located within 90°.

6. Conclusions

[42] Calculations of the abundance of material derived from the SPA melt breccia that should remain in the present surface regolith at SPA-1 have shown that this ancient material is likely to comprise a significant proportion of the regolith. This conclusion is based on estimations of how much foreign basin material has been introduced into SPA during the extended period of heavy bombardment and to what degree this material mixed with the local regolith. In

all, 36 of 48 scenarios that varied the number of basins, the estimated TC sizes of those basins, and the amount of mixing between the local and foreign material estimate that greater than 40% of the surface regolith will represent ancient SPA material. The calculations also predict that the mixed megaregolith zone will be up to 2 km deep, however, most of the scenarios predict depths of no greater than approximately 1 km. Of the 48 calculated scenarios, several are unlikely in a lunar environment, but are useful for evaluating trends of modal parameter values. Consideration of the scenarios that are most likely to reflect what might actually have occurred narrows the range of the estimated abundances of SPA material. Many realistic scenarios predict that the present regolith at SPA-1 will contain 50–80% of material derived from the SPA melt breccia, with most estimates clustering around 75%. Therefore we estimate that approximately 75% of the surface regolith is composed of material derived from the ancient SPA melt breccia, which has been modified by the normal regolith forming process. This implies that any future sample return mission to the interior of the SPA basin, with a well-selected landing site, will most likely sample abundant ancient SPA derived materials.

References

Arvidson, R., R. J. Drozd, C. M. Hohenberg, C. J. Morgan, and G. Poupeau (1975), Horizontal transport of the regolith, modification of features, and erosion rates on the lunar surface, *The Moon*, *13*, 67–79.

Belton, M. J. S., et al. (1992), Lunar impact basins and crustal heterogeneity: New western limb and farside data from Galileo, *Science*, *255*, 570–576.

Blewett, D. T., B. R. Hawke, P. G. Lucey, G. J. Taylor, R. Jaumann, and P. D. Spudis (1995), Remote sensing and geologic studies of the Schiller-Schickard region of the Moon, *J. Geophys. Res.*, *100*, 16,595–16,977.

Cintala, M. J., and R. A. F. Grieve (1994), The effects of differential scaling of impact melt and crater dimensions on lunar and terrestrial craters: Some brief examples, in *Large Meteorite Impacts and Planetary Evolution*, edited by B. O. Dressler, R. A. F. Grieve, and V. L. Sharpton, *Geol. Soc. Am. Spec. Pap.*, *293*.

Cintala, M. J., and R. A. F. Grieve (1998), Scaling impact melting and crater dimensions: Implications for the lunar cratering record, *Meteor. Planet. Sci.*, *33*, 889–912.

Cook, A. C., P. D. Spudis, M. S. Robinson, and T. R. Waters (2002), Lunar topography and basins mapped using a Clementine stereo digital elevation model [CD-ROM], *Proc. Lunar Planet. Sci. Conf., 33rd*.

Croft, S. K. (1985), The scaling of complex craters, *J. Geophys. Res.*, *90*, 828–842.

Gillis, J. J., B. L. Jolliff, and P. G. Lucey (2003), South Pole-Aitken sample return mission: Collecting mare basalts from the far side of the Moon [CD-ROM], *Proc. Lunar Planet. Sci. Conf., 34th*.

Hartmann, W. K., and C. A. Wood (1971), Moon: Origin and evolution of multi-ring basins, *The Moon*, *3*, 3–78.

Haskin, L. A., J. J. Gillis, B. L. Jolliff, and R. L. Korotev (2003a), Regolith in the South Pole-Aitken Basin is mainly indigenous material [CD-ROM], *Proc. Lunar Planet. Sci. Conf., 34th*.

Haskin, L. A., B. E. Moss, and W. B. McKinnon (2003b), On estimating contributions of basin ejecta to regolith deposits at lunar sites, *Meteor. Planet. Sci.*, *38*, 13–33.

Head, J. W., S. Murchie, J. F. Mustard, C. M. Pieters, G. Neukum, A. McEwen, R. Greeley, E. Nagel, and M. S. Belton (1993), Lunar impact basins: New data for the western limb and far side (Orientale and South Pole-Aitken Basins) form the first Galileo flyby, *J. Geophys. Res.*, *98*, 17,149–17,181.

Hodges, C. A., W. Muehlberger, R. E. Eggleton, and G. G. Schaber (1973), Geologic Setting of Apollo 16, *Proc. Lunar Conf., 4th*.

Hörz, F., R. Grieve, G. Heiken, P. Spudis, and A. Binder (1991), Lunar Surface Processes, in *Lunar Sourcebook: A Users Guide to the Moon*, edited by G. H. Heiken, D. T. Vaniman, and B. M. French, Cambridge Univ. Press, New York.

Housen, K. R., R. S. Schmidt, and K. A. Holsapple (1983), Crater ejecta scaling laws: Fundamental forms based on dimensional analysis, *J. Geophys. Res.*, *88*, 2485–2499.

Jolliff, B. L., J. J. Gillis, L. A. Haskin, R. L. Korotev, and M. A. Wieczorek (2000), Major lunar crustal terrains: Surface expression and crust-mantle origins, *J. Geophys. Res.*, *105*, 4197–4216.

Lawrence, D. J., W. C. Feldman, B. L. Barraclough, A. B. Binder, R. C. Elphic, S. Maurice, and D. R. Thomsen (1998), Global elemental maps of the Moon: The lunar prospector gamma-ray spectrometer, *Science*, *281*, 1484–1489.

Lawrence, D. J., W. C. Feldman, R. C. Elphic, R. C. Little, T. H. Prettyman, S. Maurice, P. G. Lucey, and A. B. Binder (2002), Iron abundances on the lunar surface as measured by the Lunar Prospector gamma-ray and neutron spectrometers, *J. Geophys. Res.*, *107*(E12), 5130, doi:10.1029/2001JE001530.

Li, L., and J. F. Mustard (2003), Highland contamination in lunar mare soils: Improved mapping with multiple end-member spectral mixture analysis (MESMA), *J. Geophys. Res.*, *108*(E6), 5053, doi:10.1029/2002JE001917.

Lucey, P. G., G. J. Taylor, and E. Malaret (1995), Abundance and distribution of iron on the Moon, *Science*, *268*, 1150–1153.

Lucey, P. G., G. J. Taylor, B. R. Hawke, and P. G. Spudis (1998), FeO and TiO_2 concentrations in the South Pole-Aitken basin: Implications for mantle composition and basin formation, *J. Geophys. Res.*, *103*, 3701–3708.

McGetchin, T. R., M. Settle, and J. W. Head (1973), Radial thickness variations in impact crater ejecta: Implications for Lunar basin deposits, *Earth Planet. Sci. Lett.*, *20*, 226–236.

Melosh, H. J. (1989), *Impact Cratering: A Geologic Process*, 245 pp., Oxford Univ. Press, New York.

Moore, H. J., C. A. Hodges, and D. H. Scott (1974), Multiringed basins-illustrated by Orientale and associated features, *Proc. Lunar Sci. Conf., 5th*, 71–100.

Oberbeck, V. R., R. H. Morrison, F. Horz, W. L. Quaide, and D. E. Gault (1974), Smooth plains and continuous deposits of craters and basins, *Proc. Lunar Sci. Conf., 5th*, 111–136.

Oberbeck, V. R., F. Horz, R. H. Morrison, W. L. Quaide, and D. E. Gault (1975), On the origin of the lunar smooth plains, *The Moon*, *12*, 19–54.

Petro, N. E., and C. M. Pieters (2003), How much melt breccia can be found in South Pole-Aitken Basin? [CD-ROM], *Proc. Lunar Planet. Sci., 33rd*.

Pieters, C. M., J. B. Adams, P. J. Mouginis-Mark, S. H. Zisk, M. O. Smith, J. W. Head, and T. B. McCord (1985), The nature of crater rays: The Copernicus example, *J. Geophys. Res.*, *90*, 12,393–12,413.

Pieters, C. M., S. Tompkins, J. W. Head, and P. C. Hess (1997), Mineralogy of the mafic anomaly in the South Pole-Aitken Basin: Implications for excavation of the lunar mantle, *Geophys. Res. Lett.*, *24*, 1903–1906.

Pieters, C. M., J. W. Head, L. Gaddis, B. Jolliff, and M. Duke (2001), Rock types of South Pole-Aitken Basin and extent of basaltic volcanism, *J. Geophys. Res.*, *106*, 28,001–28,022.

Pike, R. J. (1974), Ejecta from large craters on the Moon: Comments on the geometric model of McGetchin et al., *Earth Planet. Sci.*, *23*, 265–274.

Pike, R. J., and P. D. Spudis (1987), Basin ring spacing on the Moon, Mercury, and Mars, *Earth Moon Planets*, *39*, 129–194.

Ryder, G. (2002), Mass flux in the ancient Earth-Moon system and benign implications for the origin of life on Earth, *J. Geophys. Res.*, *107*(E4), 5022, doi:10.1029/2001JE001583.

Schultz, P. H. (1997), Forming the South Pole-Aitken Basin: The extreme games, *Proc. Lunar Planet. Sci., 27th*, 1259–1260.

Short, N. M., and M. L. Foreman (1972), Thickness of impact crater ejecta on the Lunar surface, *Mod. Geol.*, *3*, 69–91.

Spudis, P. D. (1993), *The Geology of Multi-Ring Impact Basins*, 263 pp., Cambridge Univ. Press, New York.

Spudis, P. D., R. A. Reisse, and J. J. Gillis (1994), Ancient multiring basin and the Moon revealed by Clementine laser altimetry, *Science*, *266*, 1848–1851.

Stoffler, D. (1985), Composition and evolution of the lunar crust in the Descartes highlands, Apollo 16, *J. Geophys. Res.*, *90*, 449–506.

Stuart-Alexander, D. E. (1978), Geologic map of the central far side of the Moon, Scale 1:5,000,000, *U.S. Geol. Surv., I-1047*.

Ulrich, G. E., C. A. Hodges, and W. R. Muehlberger (Eds.) (1981), Geology of the Apollo 16 Area, Central Lunar Highlands, *U.S. Geologic Survey, Prof. Pap., 1048*, 539 pp.

Wieczorek, M. A., and R. J. Phillips (1999), Lunar multiring basins and the cratering process, *Icarus*, *139*, 246–259.

Wieczorek, M. A., and M. T. Zuber (2001), A Serenitatis origin for the Imbrian grooves and South Pole-Aitken thorium anomaly, *J. Geophys. Res.*, *106*, 27,853–27,864.

Wilhelms, D. (1987), The Geologic History of the Moon, *U.S. Geol. Surv. Prof. Pap., 1348*, 302 pp.

Wilhelms, D. E., K. A. Howard, and H. G. Wilshire (1979), Geologic Map of the South Side of the Moon, Scale 1:5,000,000, *U.S. Geol. Surv. Misc. Invest. Series, I-1162*.

Yingst, R. A., and J. W. Head (1999), Geology of the mare deposits in South Pole-Aitken Basin as seen by Clementine UVVIS data, *J. Geophys. Res., 104*, 18,957–18,979.

Zuber, M. T., D. E. Smith, F. Lemoine, and G. A. Neumann (1994), The shape and internal structure of the Moon from the Clementine mission, *Science, 266*, 1839–1843.

———————————

N. E. Petro and C. M. Pieters, Department of Geological Sciences, Brown University, Providence, RI 02912, USA. (noah_petro@brown.edu)